This article has been accepted for publication in a future issue of this journal, but has not been fully edited. Content may change prior to final publication. Citation information: DOI 10.1109/TWC.2021.3074911, IEEE Transactions on Wireless Communications

Phase noise in modular millimeter wave massive MIMO

Maryam Eslami Rasekh*, Mohammed Abdelghany†, Upamanyu Madhow‡, Mark Rodwell§
Department of Electrical and Computer Engineering
University of California Santa Barbara
Email: {*rasekh, †mabdelghany, ‡madhow, §rodwell}@ece.ucsb.edu

***Abstract*—This paper investigates the effect of oscillator phase noise on a multiuser millimeter wave (mmWave) massive MIMO uplink as we scale up the number of base station antennas, fixing the load factor, defined as the ratio of the number of simultaneous users to the number of base station antennas. We consider a modular approach in which the base station employs an array of subarrays, or "tiles." Each tile supports a fixed number of antennas, and can therefore be implemented using a separate radio frequency integrated circuit (RFIC), with synchronization across tiles accomplished by employing a phased locked loop in each tile to synthesize an on-chip oscillator at the carrier frequency by locking on to a common lower frequency reference clock. Assuming linear minimum mean squared error (LMMSE) multiuser detection, we provide an analytical framework that can be used to specify the required power spectral density (PSD) mask for phase noise for a target system performance. Our analysis for the phase noise at the output of the LMMSE receiver indicates two distinct effects: self-noise for each user which is inversely proportional to the number of tiles, and cross-talk between users which is insensitive to the number of tiles, and is proportional to the load factor. These analytical predictions, verified by simulations for a 140 GHz system targeting a per-user data rate of 10 Gbps, show that tiling is a robust approach for scaling. Numerical results for our proposed design approach yield relatively relaxed specifications for phase noise PSD masks.**

Keywords: Phase noise, millimeter wave, THz, multiuser, massive MIMO, 5G, next generation wireless, modular, array of subarrays.

I. Introduction

The emergence of millimeter wave communication has produced unprecedented possibilities for next generation mobile networks. In addition to the large amounts of available spectrum, much of it unlicensed, the band has immense potential for spatial multiplexing. The small wavelengths (5 mm at 60 GHz, only 2 mm at 140 GHz) imply that hundreds or even thousands of antenna elements can fit on relatively small platforms, producing massive electronically steerable arrays with very small beamwidth. Most prior research in mmWave systems assumes RF beamforming, which employs one RF chain for the entire array, or hybrid beamforming, which employs a number of RF chains which is much smaller than the number of antenna elements in the array. However, advances in silicon implementations of mmWave hardware imply that, at least for a moderate number of antenna elements, it is possible to build low-cost RFICs with one RF chain for each antenna, opening up the possibility of all-digital beamforming for multiuser MIMO. In this paper, we investigate modular architectures using such RFICs as "tiles," in a regime where the number of antennas per tile is fixed, but the size of the overall antenna array is scaled up by increasing the number of tiles. We consider uplink communication wherein a mmWave base station receives simultaneous transmissions from many receivers using a digitally controlled phased array antenna, with the number of simultaneous users scaling linearly with array size. Our goal is to understand whether phase noise is a bottleneck for scaling in this scenario.

Phase noise has a distinctive effect on the performance of a communication link. While additive noise can be countered by increasing signal power, the multiplicative nature of phase noise leads to distortion that scales with signal power, and hence to performance floors that can only be alleviated by reducing oscillator noise. Since realizing low-noise oscillators is challenging at higher carrier frequencies, we are interested in how much we can relax phase noise specifications while attaining a target system-level performance. To this end, we develop in this paper a framework for analyzing the impact of phase noise in massive MIMO, modeling its propagation in the proposed tiled architecture. Each tile is controlled by a separate RF chip that performs down conversion as well as analog-to-digital conversion, alleviating the need to transport analog RF signals across the entire frontend. In order to emulate a single large array, the tiles must be synchronized in frequency and phase, meaning they need to be locked to a common reference. We are interested in massive base station arrays with hundreds of antennas (e.g., horizontally steered linear arrays with half-wavelength spacing), for which distributing a stable clock at mmWave carrier frequencies is challenging and power-inefficient. Instead, a low-frequency reference is distributed to the tiles, and is multiplied up to the carrier frequency via a PLL on each tile. Thus, the sources of phase noise in this architecture are the common low-frequency reference, and the VCOs driving the PLLs in the tiles, as depicted in Figure 1.

Concept system: While our analytical framework is general, our numerical evaluations are based on a concept system operating at a carrier frequency of 140 GHz, with common low-frequency reference at 10 GHz. We consider single carrier QPSK modulation at 5 Gbaud symbol rate, corresponding to an uncoded bit rate of 10 Gbps per user, and $N = 256$ base station antennas per sector. The load factor β, defined as the ratio of simultaneous users to antennas, varies from $\beta = \frac{1}{16}$ to $\beta = \frac{1}{2}$ (with a nominal value $\beta = \frac{1}{4}$), which corresponds to sector-level uncoded throughputs ranging from 160 Gbps to

1536-1276 (c) 2021 IEEE. Personal use is permitted, but republication/redistribution requires IEEE permission. See http://www.ieee.org/publications_standards/publications/rights/index.html for more information.
Authorized licensed use limited to: Univ of Calif Santa Barbara. Downloaded on June 24,2021 at 00:24:41 UTC from IEEE Xplore. Restrictions apply.

This article has been accepted for publication in a future issue of this journal, but has not been fully edited. Content may change prior to final publication. Citation information: DOI 10.1109/TWC.2021.3074911, IEEE Transactions on Wireless Communications

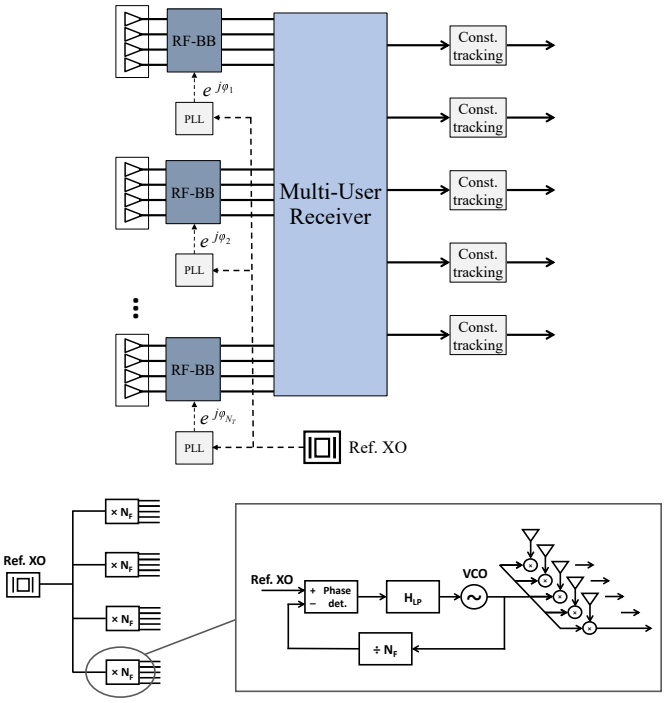

Fig. 1: Architecture of the tiled multiuser massive MIMO receiver and signal processing chain (left); schematic of two step LO generation (right).

1.28 Tbps. These aggressive specifications may well be beyond what is required in deployed systems, but they allow us to explore the limits of system performance when we impose reasonable constraints on the hardware. For the load factors of interest, spatial matched filtering does not yield acceptable performance, hence we consider LMMSE reception, arguably the simplest multiuser detection strategy we could adopt in exploring these limits.

We now summarize our contributions, and then place these in the context of prior literature.

A. Contributions

We propose the architecture depicted in Figure 1, and model the propagation of phase noise through each of the blocks depicted therein: the tile-level PLLs, the LMMSE multiuser detector, and decision-directed phase drift tracking for each user's stream at the LMMSE output. We provide a simple yet accurate model of the impact of phase noise on system performance. The resulting analytical framework is used to provide design guidelines that greatly simplify the complicated task of joint hardware/system development. This includes determining maximum allowable phase noise power spectral density (PSD) masks for oscillators so as to guarantee the desired performance level for a given system configuration.

Our focus is on the impact of phase noise on uplink demodulation, and we assume that the variations of the spatial channels for the users are much slower than the dynamics of the receiver phase noise. Thus, we assume ideal channel estimates at the base station (which might, for example, be obtained at the beginning of a frame). This enables us to compute a "naive" LMMSE receiver which does not account for, or track, subsequent variations due to phase noise. We also consider an LMMSE receiver which accounts for the statistics of the phase noise, which is what would be learnt by a continuously adaptive implementation.

In the absence of phase noise, LMMSE reception suppresses multiuser interference (and forces it to zero in the absence of noise), thus avoiding performance floors at high SNR. Phase noise, on the other hand, leads to impairments which scale with signal strength, leading to performance floors. However, our analysis shows that this performance floor can be improved by increasing the number of tiles and lowering the load factor. Indeed, a key conclusion from the scaling laws we derive is that, for a given oscillator quality, the tiled massive MIMO system is more robust to phase noise than a single-input single-output (SISO) link, and our ambitious system goals are achievable with moderate phase noise masks.

The technical approach and results that lead us to these conclusions are summarized as follows:

- Using a standard linearized model for the PLL in each tile, we show that the PLL acts as a lowpass filter for the reference phase noise, and a highpass filter for the VCO phase noise.
- The contribution of the reference phase noise at the PLL output passes unchanged through the LMMSE multiuser detector, and is highpass filtered by the constellation tracking block. This, combined with the lowpass filtering of PLLs, diminishes almost all of this component's energy, and the impact of reference phase noise on system performance becomes negligible. Performance is therefore limited by the VCO phase noise contributions at the tile PLL outputs, which is highpass.
- The performance of "naive" LMMSE and LMMSE accounting for phase noise statistics are virtually identical, which implies that continuously adaptive implementations are not required.
- Under a small phase approximation for the VCO phase noise (accurate for the design regimes that we target), we compactly characterize the LMMSE output of user k as follows (ignoring additive thermal noise in this summary):

$$y_k = e^{j\psi_k} s_k + I_k \tag{1}$$

where the output phase noise ψ_k is self-noise from user k with variance $\frac{\sigma_\phi^2}{N_T}$, and the additive noise, I_k, is cross-user interference with variance $\beta\sigma_\phi^2$, with σ_ϕ^2 denoting VCO phase noise variance at the PLL output and N_T the number of tiles. Thus, the self-noise is reduced by increasing the number of tiles, while multiuser interference is insensitive to the number of tiles, but is reduced by decreasing the load factor.

- We provide an upper bound on the error probability for QPSK in a SISO system, in terms of an effective SNR which combines the effect of additive noise, self noise, and phase noise-induced interference. We then use this to obtain an accurate approximation to the error probability for our massive MIMO model, including the effect of noise enhancement due to interference suppression.
- We provide design examples on how to determine the maximum tolerable VCO phase noise variance, σ_ϕ^2, for a desired

1536-1276 (c) 2021 IEEE. Personal use is permitted, but republication/redistribution requires IEEE permission. See http://www.ieee.org/publications_standards/publications/rights/index.html for more information.
Authorized licensed use limited to: Univ of Calif Santa Barbara. Downloaded on June 24,2021 at 00:24:41 UTC from IEEE Xplore. Restrictions apply.

This article has been accepted for publication in a future issue of this journal, but has not been fully edited. Content may change prior to final publication. Citation information: DOI 10.1109/TWC.2021.3074911, IEEE Transactions on Wireless Communications

system-level performance, and how that maps to specifications on the allowable phase noise PSD and PLL parameters. In order to allow for a simplified error correction framework with hard decisions (appropriate for the very high data rates of interest), we target an uncoded BER of 10^{-3}, which is easily handled by lightweight high-rate binary error correction codes. Numerical results show that the BER floor is well below this target in the regimes of interest.

B. Related Work

The effect of various hardware impairments (such as amplifier nonlinearity, low precision ADC and DAC, I-Q imbalance, and phase noise) on massive MIMO systems has been the subject of many modeling studies, including [1]–[5]. Among these effects, the multiplicative action of phase noise is particularly challenging to model, especially for large communication bandwidth. Significant efforts have been made by the hardware community to extract accurate models for phase noise from the physics of oscillator circuitry. Various works have utilized the framework established in [6] to develop descriptions for the phase noise generated in different configurations [7]–[12], typically by describing the PSD of the phase noise process. Modeling the overall impact of phase noise on the communication link requires a system-level analysis that incorporates such models of the phase noise into the signal reception and decoding process, as carried out in [13] for a SISO link. Most prior studies in this direction, however, have often employed oversimplified models such as the pessimistic Wiener process model considered in [14] or the white noise model assumed in [15]. Many studies neglect the possibility of leveraging time domain correlations in a phase noise process for suppressing phase drift, unnecessarily tying system performance to channel tracking overhead by relying on frequent CSI updates for drift suppression [16], whereas tracking phase drift over time is crucial in realizing the true capacity of a practical system [17]. Furthermore, most studies that consider multiple antenna systems assume either a common clock with fully correlated phase noise across the array (synchronous clock distribution), or a free-running oscillator at each element untethered to a common reference (asynchronous distribution), producing uncorrelated phase drifts at different antennas [15], [17]–[23]. The former is impractical at high carrier frequencies while the latter suffers from beamforming degradation as a result of rapid "channel aging" [23]. In [24], a two step synchronization method is implemented to avoid these drawbacks. However, the analysis therein is limited to SIMO and MISO communication where a multiple antenna base station communicates with a single user.

In terms of modeling, the closest approach to ours in the literature is that of [25], which investigates the effect of phase noise on OFDM multi-user beamforming arrays. They assume an independent oscillator at each array element locked to a common lower frequency reference via a PLL multiplier and model the filtering effects of the PLL on common and independent phase noise. In their analysis, the authors rely on a subset of subcarriers acting as pilots for phase noise tracking, and derive SINR predictions for single user and multiuser beamforming that predict similar scaling laws as our analysis. However, as shown in this and other studies, phase noise poses an inherent challenge for OFDM systems: The inter-carrier interference caused by phase noise increases with the number of subcarriers posing a fundamental limit on the bandwidth of an OFDM system impacted by phase noise [25]–[34]. OFDM also has other drawbacks for mmWave systems: the linearity required to handle high peak-to-average ratios is difficult to realize at reasonable power efficiency at high frequencies, and the precision required in analog-to-digital conversion is a challenge at large bandwidths. We therefore focus on a single carrier system in this paper. Note that, at such high frequencies, the number of significant paths in the channel is small, and beamforming with large arrays rejects multipath, thus eliminating ISI and providing a frequency-flat single path channel even at GHz bandwidths.

A key distinguishing aspect of the approach in the present paper is that it abstracts the oscillator phase noise models developed by hardware experts into a rigorous system-level framework in which the propagation of phase noise through signal processing blocks is accurately modeled. To the best of our knowledge, this is also the first paper to consider a hierarchical approach to scaling massive MIMO with a fixed number of antennas per tile. The analysis is distilled into compact scaling laws for modular MIMO which succinctly link performance to hardware and system design parameters.

The current work is a significant extension of preliminary results reported in our conference paper [35], including a more detailed theoretical treatment of phase noise scaling, introduction of BER approximations via effective SNR and SINR, derivation of LMMSE reception accounting for phase noise statistics, and validation of our analytical estimates via full system simulations.

II. System Model

We consider uplink multiuser MIMO in which the base station, equipped with an N-element digitally steered array, simultaneously receives signals sent by K users. The *load factor* is defined as the ratio of users to array size, and denoted by $\beta = K/N$.

We consider line-of-sight (LoS) channels between users and the base station. Our focus is on the impact of phase noise on multiuser demodulation rather than on channel estimation. Thus, we consider durations over which the spatial channels are well modeled as constant, and assume that the spatial channels at the beginning of such durations are known to the receiver. We discuss this assumption further in our conclusions in Section VII. The vector $\mathbf{h}_k$ represents the channel of user k, with complex amplitude g_k and angle of arrival θ_k. For ease of notation we define the *spatial frequency* corresponding to θ_k as $\omega_k = (2\pi d/\lambda)\sin\theta_k$, where d is the array inter-element spacing (half the wavelength), and λ is the carrier wavelength. User k's channel can thus be represented by the sinusoid,

$$\mathbf{h}_k = g_k \left[1, e^{j\omega_k}, e^{j2\omega_k}, \ldots, e^{j(N-1)\omega_k} \right]^T. \qquad (2)$$

For simplicity, we assume that the K spatial frequencies are distributed uniformly over $(-\pi, \pi)$ (rather than uniformly over

1536-1276 (c) 2021 IEEE. Personal use is permitted, but republication/redistribution requires IEEE permission. See http://www.ieee.org/publications_standards/publications/rights/index.html for more information.
Authorized licensed use limited to: Univ of Calif Santa Barbara. Downloaded on June 24,2021 at 00:24:41 UTC from IEEE Xplore. Restrictions apply.

This article has been accepted for publication in a future issue of this journal, but has not been fully edited. Content may change prior to final publication. Citation information: DOI 10.1109/TWC.2021.3074911, IEEE Transactions on Wireless Communications

angles of arrival). In order to limit the variation in performance across users, we assume that users that are too close in spatial frequency are orthogonalized in time or frequency domain, maintaining a minimum pairwise distance of $2\pi/N$ in spatial frequency between users. While our analytical framework easily accommodates variations in user power, we assume perfect power control on the user side ($|g_k| = 1, \forall k$) for simplicity of exposition.

For the concept system described in Section I, our nominal configuration is an $N = 256$ element array with $K = 64$ users, or $\beta = 1/4$. We consider single-carrier digital modulation with Gray coded QPSK, and use uncoded BER of 10^{-3} as our performance target, since low frame error rates can be achieved using high-rate error correction codes at this BER. We assume here that the bandwidth B (5 GHz for our concept system) equals the symbol rate $1/T_{\text{symb}}$, but the analysis easily extends to accommodate excess bandwidth. Nominal beamformed SNR (not including phase noise) is 14 dB. This provides a margin of 4 dB compared to the 10 dB required SNR for 10^{-3} BER for a SISO link without multiuser interference or phase noise. LMMSE reception is used to separate user data streams, and constellation tracking with window size of 10 is performed at the output of each channel to offset slow-time-scale oscillator phase drift. While we use uncoded BER as our performance metric here, our SINR-based analytical framework easily extends to alternative metrics such as spectral efficiency.

The modular architecture. Figure 1 depicts the modular structure of an N-element array containing N_T tiles, each with M elements, so that $N = N_T M$. In our nominal configuration, the number of tiles, N_T, is set to 16 and the number of elements on each tile is $M = 16$. We define the "underloaded" case where the number of users is no larger than the tile size, i.e., $K \leq M$ or equivalently $\beta N_T \leq 1$. In this regime, the measurements obtained from a single tile are enough for accurate reception at high SNR (e.g., with zero-forcing) and scaling laws differ significantly from the nominal mode of operation. Since our goal is to scale up the system ($K, N \to \infty$) while keeping tile size M and load factor β constant, the underloaded regime will not be the operating condition of a large system and is of limited interest for scaling.

A 10 GHz reference is distributed to tiles and frequency multiplied on-tile using a PLL-controlled VCO to produce the 140 GHz carrier. Since the phase noises at different VCOs are independent, the carriers at different tiles contain independent phase noise components. The system block diagram for this process is depicted in Figure 2. In our running example, the multiplication factor is $N_f = 14$, producing a 140 GHz carrier from the 10 GHz reference clock. The PLL is type-2 with loop resonance frequency of $\omega_n = 10$ MHz and damping factor of $\xi = 0.707$, achieved by setting

$$k_V = N_f \omega_n^2, \qquad H_{\text{LP}}(s) = \frac{1 - \frac{2\xi}{\omega_n} s}{s}. \tag{3}$$

Receiver modeling. In the absence of phase noise, the complex baseband signal received on the N-dimensional array is described by

$$\mathbf{x}_{\text{ideal}} = \mathbf{H}\mathbf{s} + \boldsymbol{\nu}, \tag{4}$$

where $\mathbf{H} = [\mathbf{h}_1 ... \mathbf{h}_K]$ is the $N \times K$ channel matrix, $\mathbf{s}$ is a K-dimensional vector containing the symbols transmitted by users, and $\boldsymbol{\nu} \sim \mathcal{CN}(\mathbf{0}, N_0 \mathbf{I}_N)$ is the additive receiver noise vector. Without loss of generality, we assume symbols are unit power ($E_s = 1$) and define the *normalized* noise power, $\sigma_\nu^2 = \frac{N_0}{E_s}$. In the presence of phase noise, the received signals on separate subarrays are distorted by different phase noise terms during down conversion. Denoting by $\mathbf{H}_i$ the $M \times K$ channel matrix of the i'th subarray, we have

$$\mathbf{H} = \begin{bmatrix} \mathbf{H}_1 \\ \mathbf{H}_2 \\ \vdots \\ \mathbf{H}_{N_T} \end{bmatrix}, \tag{5}$$

and the phase distorted received signal is modeled as

$$\mathbf{x} = e^{j\phi_0} \begin{bmatrix} \mathbf{H}_1 e^{j\phi_1} \\ \mathbf{H}_2 e^{j\phi_2} \\ \vdots \\ \mathbf{H}_{N_T} e^{j\phi_{N_T}} \end{bmatrix} \mathbf{s} + \boldsymbol{\nu} \tag{6}$$

where ϕ_i is the contribution of VCO phase noise at tile i (independent across tiles) and ϕ_0 is the reference phase noise, which is identical for all tiles. Since the additive noise, $\boldsymbol{\nu}$, is a vector of i.i.d. symmetric complex Gaussians, its distribution is rotationally symmetric and is unchanged by phase noise, hence we use the same symbol to represent its phase distorted version. A linear receiver, $\boldsymbol{\Gamma}_{K \times N}$, is used to estimate the transmitted symbols as

$$\mathbf{y} = \boldsymbol{\Gamma}\, \mathbf{x}, \tag{7}$$

which is mapped to the closest symbols in the constellation to obtain $\hat{\mathbf{s}}$. The distortion caused by phase noise on the estimated output is described in detail in later sections along with optimal linear receiver design.

III. Phase Noise Modeling

A perfectly noiseless carrier has constant complex baseband amplitude, $C(t) = A$. In a noisy setting, the complex envelope of an oscillator output becomes $C(t) = A + n(t) = A + n_c(t) + j n_s(t)$, where $n(t)$ is a complex Gaussian random process and n_c and n_s are its real and imaginary parts. For $A \gg |n(t)|$, we obtain our standard phase noise model

$$C(t) = A e^{j\phi(t)} \tag{8}$$

where $\phi(t) = \frac{n_s(t)}{A}$ is a Gaussian random process with power expressed in dBc, or dB relative to carrier power. We note that amplitude distortion is much less critical, especially as hard limiters are often used to equalize the amplitude.

As is conventional in the hardware literature, we denote the PSD of phase noise ϕ as $L(f)$. The dynamics of active components in oscillators produce *colored* phase noise in the output sinusoid [6]–[8], [13]. This phase noise is modeled as a combination of white noise and lowpass components with

1536-1276 (c) 2021 IEEE. Personal use is permitted, but republication/redistribution requires IEEE permission. See http://www.ieee.org/publications_standards/publications/rights/index.html for more information.
Authorized licensed use limited to: Univ of Calif Santa Barbara. Downloaded on June 24,2021 at 00:24:41 UTC from IEEE Xplore. Restrictions apply.

This article has been accepted for publication in a future issue of this journal, but has not been fully edited. Content may change prior to final publication. Citation information: DOI 10.1109/TWC.2021.3074911, IEEE Transactions on Wireless Communications

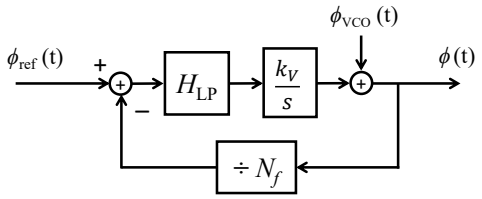

Fig. 2: LTI system model of PLL for phase noise.

PSD proportional to $1/f$, $1/f^2$, and $1/f^3$. Oscillator phase noise PSD is thus described parametrically by

$$L(f) = a_0 + \frac{a_1}{f} + \frac{a_2}{f^2} + \frac{a_3}{f^3}. \tag{9}$$

For simplicity we assume here that all clocks are unit amplitude ($A = 1$). When a noisy oscillator is used to down-convert an RF signal, the bandpass phase noise in the oscillator output is directly transferred to the demodulated baseband signal. For digital communication this translates to rotation of the baseband symbols relative to the transmitted constellation points.

A. Phase noise in the tiled array

Figure 2 shows the linearized PLL model. The signal described by this model is the *phase* of the input and output signals and therefore predicts accurately how VCO and reference phase noise are affected in the process. The phase noise at the output of this system is the sum of contributions from the reference and VCO phase noise; the former is identical in all tiles, whereas the latter is independent from one tile to another but identical over elements of the same tile. The relation between phase noise at the output of the PLL and reference and VCO phase noise is described through the model of Figure 2 as

$$\tilde{\phi}(s) = \tilde{\phi}_{\text{vco}}(s) + \frac{k_V}{s} H_{\text{LP}}(s) \left(\tilde{\phi}_{\text{ref}}(s) - \frac{\tilde{\phi}(s)}{N_f} \right) \tag{10}$$

where $\tilde{u}$ denotes the frequency domain representation (Laplace transform) of the time domain function u, and k_V is the VCO conversion gain. With some manipulation, we arrive at the PLL filters applied to each phase noise source,

$$\tilde{\phi}(s) = H_{\text{ref}}^{\text{PLL}}(s)\tilde{\phi}_{\text{ref}}(s) + H_{\text{vco}}^{\text{PLL}}(s)\tilde{\phi}_{\text{vco}}(s), \tag{11}$$

where

$$H_{\text{ref}}^{\text{PLL}}(s) = \frac{N_f k_V H_{\text{LP}}(s)}{N_f s + k_V H_{\text{LP}}(s)},$$
$$H_{\text{vco}}^{\text{PLL}}(s) = \frac{N_f s}{N_f s + k_V H_{\text{LP}}(s)}.$$

The loop filter, H_{LP}, is lowpass, therefore we observe that the PLL acts as a lowpass filter for reference phase noise and a highpass filter for VCO phase noise.

The filtering of reference phase noise by the PLL leaves only its *low frequency* components which results in a slow-varying signal that changes on a time scale of many symbols (hundreds or even thousands, depending on the filter bandwidth and symbol rate). Furthermore, this noise is constant over the array and passes through the linear receiver to the output where it can be tracked and compensated as described in the next section. We see, therefore, that the overall impact of reference phase noise on demodulation is very small. Of course, as discussed in Section VII, accounting for reference phase noise is important for channel estimation.

TABLE I: Examples of q coefficients for nominal system.

	q_0 (Hz)	q_1	q_2 (Hz^{-1})	q_3 (Hz^{-2})
$H_{\text{vco}}^{\text{PLL}}$	5×10^9	11	2.2×10^{-7}	1.6×10^{-14}
$H_{\text{ref}}^{\text{PLL}} H_W$	1.1×10^9	13	6×10^{-7}	2×10^{-13}

$\sigma_\phi^2 = 0.11, \qquad \sigma_0^2 = 2.4 \times 10^{-3}$

VCO phase noise, on the other hand, is constant for elements on one tile, but *independent over different tiles,* and therefore affects the spatial processing of multiuser detection in a nontrivial manner. We define by $\phi_i(t)$ the VCO phase noise in the carrier of tile i and derive its variance as

$$\mathbb{E}\phi_i^2 = \sigma_\phi^2 = \int_{-B/2}^{B/2} L_{\text{vco}}(f) \left| H_{\text{vco}}^{\text{PLL}}(f) \right|^2 df \tag{12}$$

where $L_{\text{vco}}(f)$ is the VCO phase noise PSD and B is the system bandwidth. As we demonstrate in upcoming discussions, the impact of phase noise on the tiled multiuser system is determined by this variance, which is a linear function of the oscillator phase noise coefficients introduced in (9), expressed as

$$\sigma_\phi^2 = \sum_{i=0}^{3} q_i a_i, \qquad q_i = \int_{-B/2}^{B/2} \frac{1}{f^i} \left| H_{\text{vco}}^{\text{PLL}}(f) \right|^2 df. \tag{13}$$

If the largest tolerable phase noise variance for a system is $\sigma_{\phi\,\max}^2$, any $L(f)$ mask that satisfies $\sum q_i a_i \le \sigma_{\phi\,\max}^2$ maintains the desired system performance. Table I reports the values of these coefficients for our nominal configuration.

We now provide a simple upper bound (Theorem 1) on the BER for Gray coded QPSK in a SISO system with both phase noise and additive noise, defining an equivalent SNR that combines the effects of both. We use this result in Section V, where we characterize the SINR in our MIMO system, to estimate the BER.

B. Equivalent SNR for SISO BER with phase noise

Consider a Gray coded QPSK signal (corresponding to independent BPSK streams along I and Q) distorted by phase noise $\varphi(t)$ and additive complex Gaussian noise $n(t)$,

$$y(t) = e^{j\varphi(t)} s(t) + n(t), \tag{14}$$

where $\mathbb{E}|s|^2 = E_s$, $\mathbb{E}|n|^2 = N_0$, and $\varphi \sim \mathcal{N}(0, \sigma_\varphi^2)$. In the absence of phase noise, the BER of this system is given by the well-known formula

$$\text{BER}_{\sigma_\varphi^2 = 0} = Q\left(\sqrt{\frac{E_s}{N_0}} \right) = Q\left(\sqrt{\text{SNR}} \right), \tag{15}$$

where $\text{SNR} := E_s/N_0$. In the absence of additive noise, on the other hand, the BER is closely approximated as

$$\text{BER}_{N_0 = 0} = Q\left(\frac{\frac{\pi}{4}}{\sigma_\varphi} \right) = Q\left(\sqrt{\text{SNR}_\varphi} \right), \tag{16}$$

1536-1276 (c) 2021 IEEE. Personal use is permitted, but republication/redistribution requires IEEE permission. See http://www.ieee.org/publications_standards/publications/rights/index.html for more information.
Authorized licensed use limited to: Univ of Calif Santa Barbara. Downloaded on June 24,2021 at 00:24:41 UTC from IEEE Xplore. Restrictions apply.

This article has been accepted for publication in a future issue of this journal, but has not been fully edited. Content may change prior to final publication. Citation information: DOI 10.1109/TWC.2021.3074911, IEEE Transactions on Wireless Communications

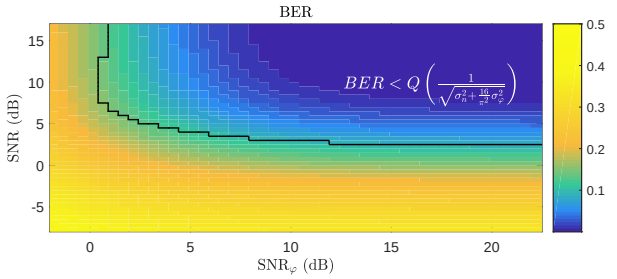

Fig. 3: BER of (14) as a function of SNR and SNR$_\varphi$. The pessimistic approximation (21) is an upper bound in the region above the solid black line, which is well within operating regimes of interest. In particular, we are in this region for SNR and SNR$_\varphi$ as low as 5 dB, and BER as high as 10%.

where we define the *phase noise SNR* as

$$\text{SNR}_\varphi = \frac{\pi^2}{16\sigma_\varphi^2}. \tag{17}$$

We now define an *equivalent SNR* obtained by adding the two distortion effects:

$$\text{SNR}_{\text{eq}}^{-1} = \text{SNR}^{-1} + \text{SNR}_\varphi^{-1}. \tag{18}$$

The following theorem states that this equivalent SNR provides a pessimistic prediction for the BER of the system described in (14) in the regimes of operation we are interested in.

Theorem 1. *The BER of the system described in (14) - (18) is upper bounded by*

$$\begin{aligned} BER < U := & \, Q\left(\sqrt{SNR_{eq}}\right) \\ & + \frac{1}{2}\left(Q\left(\sqrt{SNR}\right) - Q\left(\sqrt{SNR} + \sqrt{\frac{2SNR}{\pi SNR_\varphi}}\right)\right) \\ & + Q\left(2\sqrt{SNR_\varphi}\right). \end{aligned} \tag{19}$$

Proof. See Appendix A.

Remark 1. *At high SNR, the upper bound U is dominated by its first term, $Q(\sqrt{SNR_{eq}})$. Specifically, note that $SNR, SNR_\varphi \geq SNR_{eq}$, where the inequalities are strict when both SNR and SNR_φ are finite. It is therefore easy to see, given that $Q(x) \doteq e^{-x^2/2}$ for large x, that*[1]

$$\lim_{\substack{SNR\to\infty \\ SNR_\varphi\to\infty}} \frac{U}{Q\left(\sqrt{SNR_{eq}}\right)} = 1 \implies U \doteq Q(\sqrt{SNR_{eq}}). \tag{20}$$

Indeed, as illustrated in Figure 3, the first term in (19) is an upper bound on BER in all SNR regimes of interest to us. Thus, the overall distortion in (14) is pessimistically modeled by additive noise corresponding to SNR$_{\text{eq}}$ defined by (17) and (18), and we can use the simplified expression

$$\text{BER} \approx Q\left(\sqrt{\text{SNR}_{\text{eq}}}\right) \tag{21}$$

for deriving design guidelines. For the multiuser MIMO system that we are interested in, we replace SNR$_{\text{eq}}$ by SINR$_{\text{eq}}$.

[1]The symbol $A \doteq B$ represents asymptotic equivalence, with $\frac{\log A}{\log B} \to 1$.

IV. Multiuser Reception

For simultaneous reception of the K user signals, we employ LMMSE interference suppression followed by per-user constellation tracking, as described below.

A. LMMSE reception

Assuming phase noise terms are small (which we ensure by design for the regimes of interest), we use the approximation $e^{j\epsilon} \approx 1 + j\epsilon$ to write (6) as

$$\mathbf{x} \approx e^{j\phi_0}\mathbf{H}\mathbf{s} + \boldsymbol{\nu} + e^{j\phi_0}\begin{bmatrix} \mathbf{H}_1 j\phi_1 \\ \mathbf{H}_2 j\phi_2 \\ \vdots \\ \mathbf{H}_{N_T} j\phi_{N_T} \end{bmatrix}\mathbf{s}. \tag{22}$$

Since the common phase shift term $e^{j\phi_0}$ is seen by all users' signals, it does not affect the structure of multiuser detection. It is useful, therefore, to consider a version of the received signal with the common phase factored out, as follows:

$$\tilde{\mathbf{x}} = \mathbf{x}e^{-j\phi_0} \approx \mathbf{H}\mathbf{s} + \boldsymbol{\nu} + \begin{bmatrix} \mathbf{H}_1 j\phi_1 \\ \mathbf{H}_2 j\phi_2 \\ \vdots \\ \mathbf{H}_{N_T} j\phi_{N_T} \end{bmatrix}\mathbf{s}. \tag{23}$$

We do not change our notation for the circular complex Gaussian noise vector $\boldsymbol{\nu}$, since its distribution is rotationally invariant. We derive the LMMSE receiver for the signal model (23), and correct the common phase rotation, $e^{j\phi_0}$, after the LMMSE block. In this signal model, the VCO phase noise terms, $\{\phi_i\}$, introduce an additional distortion term to the classical multiuser reception model described by (4). In the absence of phase noise, the LMMSE receiver for model (4) is given by

$$\boldsymbol{\Gamma}_{\text{LMMSE}} = \mathbf{H}^H\left(\mathbf{H}\mathbf{H}^H + \sigma_\nu^2\mathbf{I}\right)^{-1}. \tag{24}$$

For the phase noise distorted model of (22), with the $e^{j\phi_0}$ factor set aside, we derive the LMMSE receiver by treating the channel-dependent distortion,

$$\mathbf{z} = \begin{bmatrix} \mathbf{H}_1 j\phi_1 \\ \mathbf{H}_2 j\phi_2 \\ \vdots \\ \mathbf{H}_{N_T} j\phi_{N_T} \end{bmatrix}\mathbf{s} \tag{25}$$

as an additional noise term. Assuming that the user symbols are unit power and uncorrelated, $\mathbb{E}\,\mathbf{s}\mathbf{s}^H = \mathbf{I}_K$ and the covariance matrix of this distortion is of the form

$$\mathbf{C}_z = \sigma_\phi^2\begin{bmatrix} \mathbf{H}_1\mathbf{H}_1^H & \mathbf{0} & \dots & \mathbf{0} \\ \mathbf{0} & \mathbf{H}_2\mathbf{H}_2^H & \dots & \mathbf{0} \\ \vdots & \vdots & \ddots & \vdots \\ \mathbf{0} & \mathbf{0} & \dots & \mathbf{H}_{N_T}\mathbf{H}_{N_T}^H \end{bmatrix} \tag{26}$$

where σ_ϕ^2 is the filtered VCO phase noise variance described by (12). The optimal linear receiver for a phase noise distorted system is therefore calculated as

$$\boxed{\boldsymbol{\Gamma}_{\text{LMMSE}} = \mathbf{H}^H\left(\mathbf{H}\mathbf{H}^H + \sigma_\nu^2\mathbf{I} + \mathbf{C}_z\right)^{-1}.} \tag{27}$$

1536-1276 (c) 2021 IEEE. Personal use is permitted, but republication/redistribution requires IEEE permission. See http://www.ieee.org/publications_standards/publications/rights/index.html for more information.
Authorized licensed use limited to: Univ of Calif Santa Barbara. Downloaded on June 24,2021 at 00:24:41 UTC from IEEE Xplore. Restrictions apply.

This article has been accepted for publication in a future issue of this journal, but has not been fully edited. Content may change prior to final publication. Citation information: DOI 10.1109/TWC.2021.3074911, IEEE Transactions on Wireless Communications

In terms of implementation, the naive LMMSE receiver (24) may be realized using one-shot channel estimates at the beginning of a coherence frame while the receiver of (27) may be obtained by empirical adaptation over a period long enough to capture noise statistics. If the variance of phase noise is known, the optimal receiver (27) may also be computed analytically from channel measurements (e.g., at the beginning of the frame).

B. Per-user constellation tracking

Reference phase noise is common over the array and therefore passes through the linear receiver to the output of all channels, i.e.,

$$\mathbf{y} = \mathbf{\Gamma x} = e^{j\phi_0}\mathbf{\Gamma}\tilde{\mathbf{x}}. \tag{28}$$

The common phase ϕ_0 at the output of linear multiuser detection can be tracked in decision-directed fashion. For example, letting $\hat{s}_k$ denote the hard decision for s_k, a decision-directed estimate of output phase noise is given by

$$\hat{\phi}_{\text{out}} = \angle\left(y_k \hat{s}_k^*\right). \tag{29}$$

This overall phase distortion contains highpass contributions from tile VCOs and a lowpass component that is the filtered reference phase noise, ϕ_0. By taking the averaged estimate over a W-long window of symbols, the lowpass component is isolated as

$$\hat{\phi}_0(t) = \angle\left(\sum_{i=1}^{W} y_k(t - iT_{\text{symb}})\hat{s}_k^*(t - iT_{\text{symb}})\right) \tag{30}$$

which is used to predict and undo the reference phase drift before making hard decisions for user k's symbol at time t. Assuming error-free symbol detection, this "constellation tracking" process can be abstracted as a windowed demeaning filter applied to the output phase noise, with impulse response

$$h_W(t) = \delta(t) - \frac{1}{W}\sum_{i=1}^{W}\delta(t - i\,T_{\text{symb}}) \tag{31}$$

where $T_{\text{symb}} = 1/B$ is the symbol duration. The window size, W, is a tunable design parameter; a smaller window can track phase drift faster and has a larger rejection bandwidth, but introduces greater noise enhancement at high frequencies. This effect is clearly shown in Figure 4b where the frequency response of the tracking filter is depicted for different window sizes. Constellation tracking captures the slow variations in ϕ_0, and acts as a highpass filter for the common phase noise. On the other hand, as noted earlier, the tile PLLs act as lowpass filters for the common phase. This cascade therefore diminishes almost all of the reference phase noise power. The variance of the residual reference phase noise can now be computed using the abstracted tracking model as

$$\boxed{\mathbb{E}\phi_0^2 = \sigma_0^2 = \int_{-B/2}^{B/2} L_{\text{ref}}(f)\left|H_{\text{ref}}^{\text{PLL}}(f)H_{\text{W}}(f)\right|^2 df} \tag{32}$$

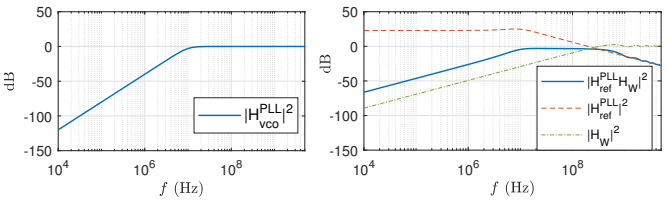

(a)

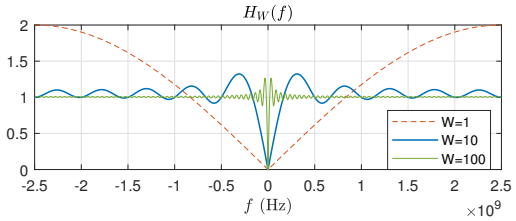

(b)

Fig. 4: (a) Effective filters applied to VCO and reference phase noise in the PLL. (b) Frequency response of constellation tracking filter for different window sizes (with respect to phase signal). $W = 1$ is equivalent to differential modulation.

which depends on the filtering bandwidths of the PLL and constellation tracking process. This value is reported in Table I for the nominal configuration along with the total filtering coefficients applied to the a_i components of $L_{\text{ref}}(f)$ satisfying $\sigma_0^2 = \sum_{i=0}^{3} q_i a_i$. The filtering effects of PLL and derotation on VCO and reference phase noise are depicted in Figure 4a.

We also note that, although not explicitly indicated in the notation, the transmitted symbol s_k will contain the phase drift from the kth transmitter's local oscillator. The per-user constellation tracking at the output of the multiuser detector automatically tracks and corrects the low-frequency portion of this phase drift as well, thus automatically maintaining frequency synchronization for each user in a manner that is decoupled from multiuser detection.

The impact of constellation tracking on the per-tile VCO phase noise is less significant, as this is already a highpass signal. This impact is slight noise enhancement at the higher end of the spectrum (evident in Figure 4b) which, in our running example, increases output VCO phase noise power by about 0.7%. If the bandwidth of H_{vco}^{PLL} is smaller than that of H_W, constellation tracking may *decrease* the output VCO phase noise variance. It is worth noting that constellation tracking has no effect on the *cross-user* interference caused by VCO phase noise since it is applied *after* multiuser reception where crosstalk is produced.

V. Interference Analysis

Without loss of generality, we base our interference analysis on the signal model (23) with common phase factored out. For this model, the output of linear receiver $\mathbf{\Gamma}$ is approximated by

$$\mathbf{y} \approx \mathbf{\Gamma H s} + \mathbf{\Gamma}\boldsymbol{\nu} + \sum_{i=1}^{N_T} j\phi_i \mathbf{\Gamma}_i \mathbf{H}_i \mathbf{s} \tag{33}$$

where $\mathbf{\Gamma}_i$ denotes the i'th $K \times M$ block of $\mathbf{\Gamma}$. That is,

$$\mathbf{\Gamma} = [\mathbf{\Gamma}_1\, \mathbf{\Gamma}_2 \ldots \mathbf{\Gamma}_{N_T}]. \tag{34}$$

1536-1276 (c) 2021 IEEE. Personal use is permitted, but republication/redistribution requires IEEE permission. See http://www.ieee.org/publications_standards/publications/rights/index.html for more information.
Authorized licensed use limited to: Univ of Calif Santa Barbara. Downloaded on June 24,2021 at 00:24:41 UTC from IEEE Xplore. Restrictions apply.

This article has been accepted for publication in a future issue of this journal, but has not been fully edited. Content may change prior to final publication. Citation information: DOI 10.1109/TWC.2021.3074911, IEEE Transactions on Wireless Communications

The naive LMMSE receiver (24) focuses on suppression of the coherent (across tiles) interference in the first term. For our nominal load factor of $\beta = \frac{1}{4}$, and under the assumed minimum spatial frequency separation of $2\pi/N$, the resulting LMMSE receiver does not lead to a significant attenuation of the desired signal. The LMMSE receiver (27) does much the same, since the phase noise causing the third term is significantly smaller than the coherent interference (as $\phi_i \ll 1$). Furthermore, the third term is not coherent across tiles ($\{\phi_i\}$ are independent), and a zero-forcing receiver that satisfies $\mathbf{\Gamma}_{\text{ZF}}\mathbf{H} = \alpha\mathbf{I}_K$, does not zero out the cross-user interference in this term, as $\mathbf{\Gamma}_{\text{ZF},i}\mathbf{H}_i \neq \alpha\mathbf{I}_K$ and therefore $\sum j\phi_i\mathbf{\Gamma}_{\text{ZF},i}\mathbf{H}_i \neq \alpha\mathbf{I}_K$. Of course, in the highly underloaded regime where $K \leq M$, tile level zero-forcing is possible and, as our simulations show, the optimal receiver will in fact converge to per-tile zero forcing as SNR grows large. In the scaling regime of interest to us, K grows with array size while M stays constant, therefore tile-level interference suppression is not feasible. We estimate per-tile interference, therefore, under the following approximation.

Approximation: *At the tile-level, both LMMSE variants are assumed to be approximately aligned with the spatial matched filters:*

$$\mathbf{\Gamma}_i \approx \frac{1}{N}\mathbf{H}_i^H \tag{35}$$

Numerical verification: We have verified this approximation via extensive Monte Carlo simulations over many realizations of the channel in different (non-underloaded) regimes, but report only an example result: at our nominal SNR of 14 dB, the normalized correlation between the LMMSE receiver and the spatial matched filter, *at the tile level*, is found to exceed 0.97 with probability 99%.

Under the approximation (35), the strength of the diagonal entries of the subarray receiver output are equal to

$$|\,(\mathbf{\Gamma}_i\mathbf{H}_i)_{k,k}\,| = \frac{M}{N} \tag{36}$$

and the off-diagonal entries are zero-mean with variance

$$\mathbb{E}\left|(\mathbf{\Gamma}_i\mathbf{H}_i)_{k,l}\right|^2 = \frac{M}{N^2}, \qquad (k \neq l) \tag{37}$$

with the randomness caused by random positioning of users in the cell. We can now state the following result.

Theorem 2. *Under the approximation (35), VCO phase noise causes multiplicative self-noise and additive cross-user interference described by*

$$\boxed{y_k \approx \gamma e^{j\psi}s_k + I} \tag{38}$$

where

$$\boxed{\mathbb{E}\psi^2 = \frac{\sigma_\phi^2}{N_T}, \quad \mathbb{E}\gamma = 1 - \frac{1}{2}\sigma_\phi^2, \quad \mathbb{E}|I|^2 = \frac{K-1}{N}\sigma_\phi^2 \approx \beta\sigma_\phi^2.} \tag{39}$$

Proof. Setting aside the reference phase noise and additive thermal noise,

$$\mathbf{y} = \mathbf{\Gamma}\begin{bmatrix}\mathbf{H}_1 e^{j\phi_1}\\ \mathbf{H}_2 e^{j\phi_2}\\ \vdots \\ \mathbf{H}_{N_T} e^{j\phi_{N_T}}\end{bmatrix}\mathbf{s}. \tag{40}$$

The output of channel k is a combination of contributions from the desired and interfering users which we separate as

$$y_k = \left(\sum_{i=1}^{N_T}(\mathbf{\Gamma}_i\mathbf{H}_i)_{k,k}e^{j\phi_i}\right)s_k + \sum_{l\neq k}\left(\sum_{i=1}^{N_T}(\mathbf{\Gamma}_i\mathbf{H}_i)_{k,l}e^{j\phi_i}\right)s_l.$$

The multiplicative self-noise is derived using the first and third order Taylor expansions of sine and cosine functions, respectively, as

$$\begin{aligned}\sum_{i=1}^{N_T}(\mathbf{\Gamma}_i\mathbf{H}_i)_{k,k}e^{j\phi_i} &\approx \frac{M}{N}\sum_{i=1}^{N_T}(\cos\phi_i + j\sin\phi_i)\\ &\approx \frac{1}{N_T}\sum_{i=1}^{N_T}(1-\frac{1}{2}\phi_i^2) + j\phi_i\\ &\approx \left(1 - \frac{1}{2N_T}\sum_{i=1}^{N_T}\phi_i^2\right) + j\left(\frac{1}{N_T}\sum_{i=1}^{N_T}\phi_i\right)\\ &= \gamma + j\psi \approx \gamma e^{j\psi}\end{aligned} \tag{41}$$

where $\gamma = 1 - \frac{1}{2N_T}\sum_{i=1}^{N_T}\phi_i^2$ is an average of identically distributed non-zero-mean variables, and is therefore well-approximated by its expected value, $\gamma \approx \mathbb{E}\gamma = 1 - \frac{\sigma_\phi^2}{2}$ and $\psi = \frac{1}{N_T}\sum_{i=1}^{N_T}\phi_i$ is an average of zero-mean i.i.d. Gaussian random variables, with variance $\mathbb{E}\psi^2 = \frac{\sigma_\phi^2}{N_T}$.

We evaluate cross-user interference by using the small-phase approximation (first order Taylor expansion of e^x) to obtain

$$\begin{aligned}\sum_{i=1}^{N_T}(\mathbf{\Gamma}_i\mathbf{H}_i)_{k,l}\,e^{j\phi_i} &= \sum_{i=1}^{N_T}(\mathbf{\Gamma}_i\mathbf{H}_i)_{k,l} + \sum_{i=1}^{N_T}j\phi_i(\mathbf{\Gamma}_i\mathbf{H}_i)_{k,l}\\ &= (\mathbf{\Gamma}\mathbf{H})_{k,l} + \sum_{i=1}^{N_T}j\phi_i(\mathbf{\Gamma}_i\mathbf{H}_i)_{k,l}\\ &\approx \sum_{i=1}^{N_T}j\phi_i(\mathbf{\Gamma}_i\mathbf{H}_i)_{k,l}\end{aligned} \tag{42}$$

with $(\mathbf{\Gamma}\mathbf{H})_{k,l} \approx 0$ resulting from the LMMSE receiver effectively suppressing cross terms in $\mathbf{\Gamma}\mathbf{H}$ using all N degrees of freedom. The covariance of cross-user interference is thus found to be

$$\begin{aligned}\mathbb{E}|I|^2 &= \mathbb{E}\left|\sum_{l\neq k}\left(\sum_{i=1}^{N_T}(\mathbf{\Gamma}_i\mathbf{H}_i)_{k,l}e^{j\phi_i}\right)s_l\right|^2\\ &= (K-1)\,N_T\,\sigma_\phi^2\,\mathbb{E}|(\mathbf{\Gamma}_i\mathbf{H}_i)_{k,l}|^2\\ &= (K-1)\,\frac{N_T M}{N^2}\,\sigma_\phi^2 = \frac{K-1}{N}\sigma_\phi^2 \approx \beta\sigma_\phi^2\end{aligned} \tag{43}$$

□

1536-1276 (c) 2021 IEEE. Personal use is permitted, but republication/redistribution requires IEEE permission. See http://www.ieee.org/publications_standards/publications/rights/index.html for more information.
Authorized licensed use limited to: Univ of Calif Santa Barbara. Downloaded on June 24,2021 at 00:24:41 UTC from IEEE Xplore. Restrictions apply.

This article has been accepted for publication in a future issue of this journal, but has not been fully edited. Content may change prior to final publication. Citation information: DOI 10.1109/TWC.2021.3074911, IEEE Transactions on Wireless Communications

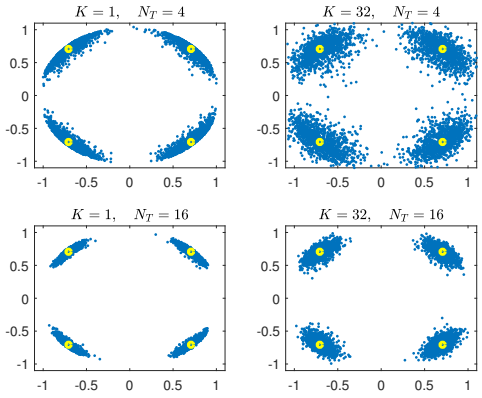

Fig. 5: Scatter plot of received QPSK symbols on a 256-element array for different load factors and number of tiles. The output phase noise decreases as number of tiles increases and interference is proportional to number of users (additive noise set to zero).

Accounting for all multiplicative and additive noise terms in the system, we arrive at the following model for the output signal:

$$y_k = \gamma e^{j(\psi+\phi_0)} s_k + I + \nu' \tag{44}$$

where

$$\gamma = 1 - \frac{\sigma_\phi^2}{2}, \qquad \mathbb{E}\psi^2 = \frac{\sigma_\phi^2}{N_T}, \qquad \mathbb{E}\phi_0^2 = \sigma_0^2,$$

$$\mathbb{E}I^2 = \beta\sigma_\phi^2, \qquad \mathbb{E}|\nu'|^2 = \frac{\sigma_\nu^2}{N}.$$

Figure 5 shows scatter plots of the received QPSK symbols in the I-Q plane for different values of K and N_T. Based on the preceding analysis, if load factor and tile size are kept constant, phase noise is not a bottleneck in scaling to larger arrays. The cross-user interference caused by phase noise only depends on the ratio of users to array size and is therefore constant, while output phase noise variance *decreases* as the number of tiles grows. In fact, we expect performance to *improve* as the system is scaled up, as long as loading, tile size, oscillator PSD, modulation, and beamformed SNR (N/σ_ν^2) are fixed.

Predicting the BER of a phase-distorted system. It is convenient to model signal attenuation via noise amplification, normalizing output signal power to unity. The equivalent normalized variance for our tiled system can be determined using Theorem 1 to be:

$$\sigma_{\text{eq}}^2 = \frac{1}{(1-\frac{1}{2}\sigma_\phi^2)^2}\left(\frac{\sigma_\nu^2}{N} + \beta\sigma_\phi^2 + \frac{16}{\pi^2}\left(\frac{\sigma_\phi^2}{N_T} + \sigma_0^2\right)\right). \tag{45}$$

This value is an *expectation* across randomly placed users, and the true realization of SINR will vary across users. Since we assume power leveling, this variation is primarily due to variations in cross-user interference. In order to provide a pessimistic prediction, we substitute the average cross-talk power $\beta\sigma_\phi^2$ with a value which is 3 standard deviations above its mean:

$$\left(\beta + 3\,\frac{0.82\sqrt{\beta}}{N_T}\right)\sigma_\phi^2 \tag{46}$$

with the constant 0.82 reflecting the upper bound limit of the standard deviation of the Dirichlet kernel, i.e.,

$$\lim_{M\to\infty} \sqrt{\mathbb{E}_{\delta\sim\mathcal{U}(-\pi,\pi)}\left(\left(\frac{\sin M\delta/2}{M\sin\delta/2}\right)^2 - \frac{1}{M}\right)^2 M} \approx 0.82.$$

Due to the rapid decay of the Q function, BER is dominated by the worst-case, and we expect this pessimistic approach to be close to the average BER. The equivalent SINR is thus modified to

$$\boxed{\sigma_{\text{eq}}^2 = \frac{1}{(1-\frac{1}{2}\sigma_\phi^2)^2}\left(\frac{\sigma_\nu^2}{N} + (\beta + 2.46\frac{\sqrt{\beta}}{N_T})\sigma_\phi^2 + \frac{16}{\pi^2}\left(\frac{\sigma_\phi^2}{N_T} + \sigma_0^2\right)\right).} \tag{47}$$

We now account for the reduction in SINR due to the reduction in signal power (modeled equivalently as noise enhancement) caused by suppression of the coherent interference. At moderate load factors (e.g., $\beta = 1/4$) and SNRs, this SINR penalty is well (and pessimistically) approximated by that due to a zero-forcing receiver. Let ρ denote the normalized cross-correlation between the spatial channels for two randomly chosen users. If the spatial frequencies are uniform over $(-\pi, \pi)$, then $E[|\rho|^2] = \frac{1}{N}$ (see Appendix B). When we enforce a minimum spatial frequency separation of $2\pi/N$, we can actually show that $E[|\rho|^2] \leq \frac{0.1}{N}$ (again, see Appendix B). In order to evaluate the impact of scaling, therefore, we set

$$E[|\rho|^2] = \frac{\alpha}{N} \tag{48}$$

where α is a factor that depends on the minimum spatial separation (or, more generally, the distribution of users' relative spatial frequencies), equal to 0.1 in our system model. Now, denoting by ρ_{lk} the normalized cross-correlation between the spatial responses for users l and k, the output *signal* power, S, of LMMSE (normalized to the matched filter output power) is bounded, using (48), as follows

$$\begin{aligned} S &\geq 1 - \sum_{l\neq k} |\rho_{lk}|^2 \\ &\implies \mathbb{E}S \geq 1 - (K-1)E[|\rho|^2] \geq 1 - \alpha\beta \end{aligned} \tag{49}$$

which, by virtue of the law of large numbers, is accurate as $K, N \to \infty$ with β fixed. Using the right-hand side of (49) as an approximation, we obtain the following pessimistic prediction of the equivalent SINR and resulting BER.

$$\boxed{\text{SINR}_{\text{eq}} \approx \frac{1-\alpha\beta}{\sigma_{\text{eq}}^2}, \qquad \text{BER}_{\text{QPSK}} \approx Q\left(\sqrt{\text{SINR}_{\text{eq}}}\right).} \tag{50}$$

This prediction, with $\alpha = 0.1$ in (50), is expected to be accurate in our regime of interest of $K > M$ and moderate SNR. In the underloaded regime, per-tile interference suppression becomes feasible and, at high enough SNR, partial per-tile interference suppression is incentivized even for $K > M$. In such settings (not of interest in our scaling regime), our

1536-1276 (c) 2021 IEEE. Personal use is permitted, but republication/redistribution requires IEEE permission. See http://www.ieee.org/publications_standards/publications/rights/index.html for more information.
Authorized licensed use limited to: Univ of Calif Santa Barbara. Downloaded on June 24,2021 at 00:24:41 UTC from IEEE Xplore. Restrictions apply.

This article has been accepted for publication in a future issue of this journal, but has not been fully edited. Content may change prior to final publication. Citation information: DOI 10.1109/TWC.2021.3074911, IEEE Transactions on Wireless Communications

prediction is *overly* pessimistic, and performance can be significantly better than predicted.

In the next section we summarize our design framework, and provide simulation results to validate our analytical predictions.

VI. Numerical Results

The models presented in this paper can be used to provide an **analytical cross-layer design framework** using four key observations.

- The reference oscillator phase noise is filtered by the PLL and constellation tracking filters and appears at the output of all channels with variance $\sigma_0^2 = \int L_{\text{ref}}(f) \left| H_{\text{ref}}^{\text{PLL}}(f) H_W(f) \right|^2 df$.
- VCO noise is filtered by the PLL resulting in tile phase noise with variance $\sigma_\phi^2 = \int L_{\text{VCO}}(f) \left| H_{\text{vco}}^{\text{PLL}}(f) \right|^2 df$. At the receiver output this produces phase noise of variance σ_ϕ^2/N_T and additive interference of power $\beta\sigma_\phi^2$.
- System performance is determined by parameters σ_0^2, σ_ϕ^2, N_T, β, and σ_ν^2/N (beamformed SNR). A pessimistic prediction is given by the equivalent SINR

$$\text{SINR}_{\text{eq}} = \frac{1-\alpha\beta}{\sigma_{\text{eq}}^2},$$

$$\sigma_{\text{eq}}^2 = (1-\sigma_\phi^2)^{-2}\left(\text{SNR}^{-1} + (\beta + \frac{2.46\sqrt{\beta}}{N_T})\sigma_\phi^2 + \frac{16}{\pi^2}\left(\frac{\sigma_\phi^2}{N_T} + \sigma_0^2\right)\right),$$

  where $\alpha = 0.1$ for the specifications of our system model.
- Permissible phase noise PSD can be expressed as a *linear constraint* on the $L(f)$ coefficients,

$$\sum q_i a_i \le \sigma_\phi^2 \text{ or } \sigma_0^2, \tag{51}$$

  with q factors obtained by (13).

Using the preceding guidelines, trade-offs between different design choices are modeled as simple analytical relationships that predict system performance with reasonable accuracy. In this section we provide numerical validation for the above framework and examine the scaling laws derived from it. The nominal system configuration is summarized in Table II.

We first provide an example of an acceptable **phase noise mask** for our nominal system specifications. We use the model of (9) to generate phase noise signals. The reference phase noise PSD is a factor of N_f lower than that of the VCO. In practice, the reference is likely to be a high quality crystal resonance oscillator with very low phase noise. The shape of the curve (a_i parameters) is chosen such that low-pass components have approximately equal contribution ($a_1 q_1 = a_2 q_2 = a_3 q_3$), and the same combined impact as the constant component for our nominal system ($a_0 q_0 = a_1 q_1 + a_2 q_2 + a_3 q_3$). Figure 6 shows the resulting $L(f)$ mask which indicates feasible phase noise requirements for our target system, as THz oscillators with lower $L(f)$ have been reported in the literature [36].

Using the PSD curve shown in Figure 6, we isolate the two distortion terms described in Theorem 2 as follows. To measure **self-noise**, we set up the end-to-end multiuser system with $\beta = 1/4$ and LMMSE reception (as described in Section IV). We then set the transmitted symbol, $s_k(t)$, to zero for all but one user throughout each simulation sequence and set the additive noise to zero (but use the nominal value for σ_ν^2 in deriving the LMMSE receiver). Figure 7 depicts self-noise for the designated user as a function of tile size and phase noise variance for a 256-element array. The analytical predictions are also plotted for comparison. We observe that simulation results follow the analytical prediction closely, and the diversity provided by independent VCOs reduces the output phase distortion.

To isolate the **cross-user interference**, we perform a similar simulation but this time set the designated user's signal to zero while all other users remain active. This way we only

TABLE II: Nominal simulation configuration

Parameter:	N	M	N_T	β	f_c	N_f	B
Value:	256	16	16	$\frac{1}{4}$	140 GHz	14	5 GHz

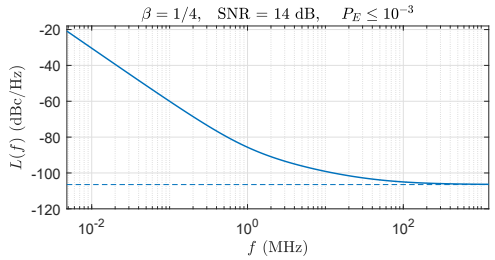

Fig. 6: Acceptable VCO phase noise mask for BER $< 10^{-3}$ and 10 Gbps rate in nominal system. Parameters: $a_0 = 2.25 \times 10^{-11}$ W/Hz, $a_1 = 9 \times 10^{-4}$ W, $a_2 = 9 \times 10^2$ WHz, $a_3 = 9 \times 10^8$ WHz^2.

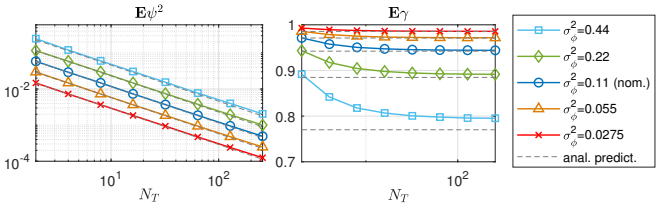

Fig. 7: Self interference phase noise and amplitude attenuation for 256 element array with 64 users. Dashed lines depict analytical predictions of $\frac{\sigma_\phi^2}{N_T}$ (left) and $1 - \frac{\sigma_\phi^2}{2}$ (right).

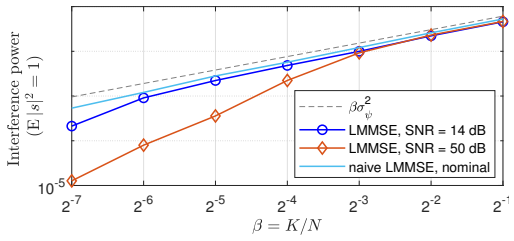

Fig. 8: Scaling of cross-talk with load factor.

1536-1276 (c) 2021 IEEE. Personal use is permitted, but republication/redistribution requires IEEE permission. See http://www.ieee.org/publications_standards/publications/rights/index.html for more information.
Authorized licensed use limited to: Univ of Calif Santa Barbara. Downloaded on June 24,2021 at 00:24:41 UTC from IEEE Xplore. Restrictions apply.

This article has been accepted for publication in a future issue of this journal, but has not been fully edited. Content may change prior to final publication. Citation information: DOI 10.1109/TWC.2021.3074911, IEEE Transactions on Wireless Communications

get cross-user interference signal at the designated output, the variance of which is the interference power. In Figure 8 we report the cross-user interference variance averaged over many realizations for naive LMMSE (that ignores the effect of phase noise) and optimal LMMSE for nominal and high SNR. Both receivers follow the analytical prediction, $\mathbb{E}|I|^2 = \beta\sigma_\phi^2$, fairly closely in most regimes. For an underloaded system at high SNR, analytical results overestimate interference for LMMSE reception since *per tile* interference suppression becomes possible, as discussed in Section V.

Full system simulations that include the effects of VCO and reference phase noise, as well as realistic implementation of constellation tracking were performed to quantify the effect of system parameters on performance. Figure 9a depicts performance as a function of tile size for various choices of load factor, assuming beamformed SNR of 14 dB and phase noise PSD depicted in Figure 6. When the array is divided into a larger number of tiles, self-noise is suppressed and BER decreases, but if β remains constant the cross-user interference does not change with N_T and therefore creates a performance floor. In Figure 9b we depict the same results for a high SNR system. As expected, we see that BER is overestimated considerably for optimal LMMSE reception in the underloaded regime. In both of these cases, we see that the fully synchronized case, corresponding to $N_T = 1$, suffers more from phase noise than any of the tiled structures and has the highest BER. This indicates that, even if distributing the carrier directly is practically possible, a tiled structure is still preferable and improves the overall performance.

Finally, Figure 10 shows how performance scales with beamformed link SNR in the presence and absence of phase noise. The performance floor caused by phase noise, especially its cross-user interference effect, is clearly visible in this figure. This floor can only be suppressed by reducing the load factor as shown in Figure 9. By comparing realistic drift tracking with the idealized model of (32) we see that, at low SINR, a decoding error can deteriorate tracking performance and cause additional errors in consecutive symbols. This effect can be mitigated by adding a margin to the target SINR. For our nominal setup, idealized performance is recovered with 0.5 dB higher SINR, which is achieved by scaling down all noise terms uniformly, i.e., increasing SNR and reducing $L(f)$ each by 0.5 dB (not depicted here). As expected, our analytical predictions are only pessimistic for the idealized case and may underestimate BER for a realistic system at low SINR.

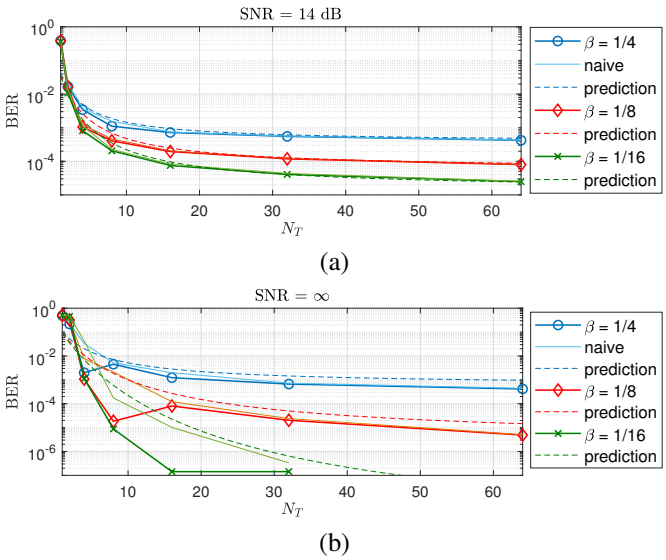

Fig. 9: Full system simulation results for the nominal configuration using $L(f)$ function of Figure 6 varying load factor and number of tiles ($N = 256$ fixed). Optimal LMMSE, naive LMMSE (ignoring phase noise; solid narrow lines), and prediction of (50) plotted for comparison.

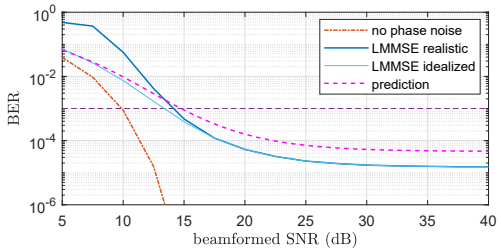

Fig. 10: Performance (BER) as a function of SNR with and without phase noise. Solid narrow curve (light blue) assuming idealized constellation tracking, i.e., no error propagation.

VII. Conclusions

Our analytical framework implies that, as far as the performance floor due to phase noise is concerned, a modular architecture with fixed-size tiles can be used to scale all-digital mmWave multiuser MIMO up arbitrarily by increasing the number of tiles, keeping oscillator noise characteristics, bandwidth and load factor fixed. A naive LMMSE receiver that employs one-shot channel estimates while ignoring phase noise, along with constellation tracking at the output, is found to work well. Our analysis provides specific guidelines to hardware designers on permissible phase noise PSD characteristics, and the specifications corresponding to our concept system are achievable in low-cost silicon processes. While the discussion here has been limited to uplink communication, analogous arguments can be made for downlink transmission. While LMMSE precoding is not as straightforward to compute as LMMSE reception, similar bounds and scaling laws can be shown to hold in downlink with (suboptimal) zero-forcing precoding. Detailed treatment of MU-MIMO downlink is left for future study.

While the scaling laws in Theorem 2 apply to arbitrary constellations (e.g., see numerical results for 16QAM in our preliminary results [35]), the BER estimates based on Theorem 1 are specialized to Gray coded QPSK. Extension of such estimates for larger constellations is an interesting topic for future work. While our analysis focuses on the impact of phase noise on demodulation, assuming ideal one-shot channel estimates are available, it is important to investigate how phase noise affects channel estimation. We expect reference phase noise to become more significant, since we can no longer count on attenuation due to post-demodulation constellation tracking. Such explorations are best undertaken in the context of specific

1536-1276 (c) 2021 IEEE. Personal use is permitted, but republication/redistribution requires IEEE permission. See http://www.ieee.org/publications_standards/publications/rights/index.html for more information.
Authorized licensed use limited to: Univ of Calif Santa Barbara. Downloaded on June 24,2021 at 00:24:41 UTC from IEEE Xplore. Restrictions apply.

This article has been accepted for publication in a future issue of this journal, but has not been fully edited. Content may change prior to final publication. Citation information: DOI 10.1109/TWC.2021.3074911, IEEE Transactions on Wireless Communications

receiver architectures. For example, the training period, and hence the impact of phase noise, can be significantly reduced by beamspace techniques which exploit the sparsity of the mmWave channel, as indicated in preliminary results reported in [37].

The results here, along with analogous results regarding the impact of nonlinearities [1], indicate that hardware impairments such as phase noise and nonlinearities do not represent fundamental bottlenecks for scaling all-digital mmWave MIMO, and provide specific design guidelines for hardware front end design. Of course, building RF hardware based on these design prescriptions is a significant challenge, as is management of the complexity of digital signal processing as bandwidth, number of antennas, and number of simultaneous users, scale up. Again, beamspace techniques [37], [38] represent a promising framework for this purpose.

ACKNOWLEDGEMENTS

This work was supported in part by ComSenTer, one of six centers in JUMP, a Semiconductor Research Corporation (SRC) program sponsored by DARPA.

APPENDIX A
PROOF OF THEOREM 1

Gray coded QPSK corresponds to independent bits sent along I and Q. By symmetry, we focus, without loss of generality, on the probability of error in the I bit when transmitting $s = e^{j\frac{\pi}{4}}$. Consider system 1 and system 2 with signal models

$$y_1 = se^{j\varphi} + n, \qquad y_2 = s + n_\varphi + n,$$

where $\varphi \sim \mathcal{N}(0, \sigma_\phi^2)$ and $n_\varphi \sim \mathcal{CN}(0, \frac{16}{\pi^2}\sigma_\phi^2)$. An error occurs in the I bit when y crosses the vertical boundary into the region $\mathfrak{Re}(y) < 0$. In the two signal models, this happens when

$$\mathfrak{Re}(y_1) = \cos\left(\frac{\pi}{4} + \varphi\right) + n_i < 0, \tag{52}$$

$$\mathfrak{Re}(y_2) = \frac{1}{\sqrt{2}} + \mathfrak{Re}(n_\varphi) + n_i < 0, \tag{53}$$

where n_i is the real part of the complex Gaussian variable n. To compare the probability of these two occurrences, we define the additive variable as $\mathfrak{Re}(n_\varphi) = -\frac{\sqrt{8}}{\pi}\varphi$ which is a zero-mean Gaussian with variance $\frac{8}{\pi^2}\sigma_\varphi^2$. Since $p(\varphi \geq 0) = p(\varphi < 0) = \frac{1}{2}$, error probabilities can be expressed as

$$\begin{aligned} P(e) &= \frac{1}{2}P\left(e|\varphi \geq 0\right) + \frac{1}{2}P\left(e|\varphi < 0\right) \\ &= \int_0^\infty P\left(e|\varphi\right)p(\varphi)d\varphi + \int_{-\infty}^0 P\left(e|\varphi\right)p(\varphi)d\varphi. \end{aligned}$$

For system 1 and system 2 we have

$$P_1(e|\varphi) = Q\left(\frac{\cos(\frac{\pi}{4}+\varphi)}{\frac{1}{\sqrt{2}}\sigma_n}\right), \; P_2(e|\varphi) = Q\left(\frac{\frac{1}{\sqrt{2}} - \frac{\sqrt{8}}{\pi}\varphi}{\frac{1}{\sqrt{2}}\sigma_n}\right),$$

where $\sigma_n^2 = N_0/E_s$ is the normalized additive noise variance. For any $\varphi \in [0, \frac{\pi}{4}]$, it holds that

$$\cos\left(\frac{\pi}{4} + \varphi\right) \geq \frac{1}{\sqrt{2}} - \frac{\sqrt{8}}{\pi}\varphi \implies P_1(e|\varphi) - P_2(e|\varphi) \leq 0$$

and, due to symmetry between $\varphi \in [0, \frac{\pi}{4}]$ and $\varphi \in [\frac{\pi}{4}, \frac{\pi}{2}]$,

$$P_1\left(e|\frac{\pi}{2} - \varphi\right) = 1 - P_1(e|\varphi), \quad P_2\left(e|\frac{\pi}{2} - \varphi\right) = 1 - P_2(e|\varphi)$$

$$\implies P_1\left(e|\frac{\pi}{2} - \varphi\right) - P_2\left(e|\frac{\pi}{2} - \varphi\right) = -(P_1(e|\varphi) - P_2(e|\varphi))$$

therefore,

$$\begin{aligned} &\left(P_1\left(e|\varphi \in [0, \frac{\pi}{2}]\right) - P_2\left(e|\varphi \in [0, \frac{\pi}{2}]\right)\right) p\left(\varphi \in [0, \frac{\pi}{2}]\right) \\ &= \int_0^{\frac{\pi}{2}} (P_1(e|\varphi) - P_2(e|\varphi))p(\varphi)d\varphi \\ &= \int_0^{\frac{\pi}{4}} \left(P_1(e|\varphi) - P_2(e|\varphi)\right)\left(p(\varphi) - p\left(\frac{\pi}{2} - \varphi\right)\right)d\varphi < 0 \end{aligned}$$

since, in the latter interval, $0 \leq \varphi \leq \frac{\pi}{4} \leq \frac{\pi}{2} - \varphi \leq \frac{\pi}{2}$ and therefore $p(\varphi) - p\left(\frac{\pi}{2} - \varphi\right) \geq 0$ while $P_1(e|\varphi) - P_2(e|\varphi) \leq 0$. Meanwhile, for $\varphi > \frac{\pi}{2}$, we have $\frac{1}{\sqrt{2}} - \frac{\sqrt{8}}{\pi}\varphi < \cos\left(\frac{\pi}{4} + \varphi\right)$ and $P_1(e|\varphi) < P_2(e|\varphi)$. We can therefore conclude that

$$P_1(e|\varphi > 0) < P_2(e|\varphi > 0).$$

For negative values of φ we have the following bounds. In system 1, for any value of $-\frac{\pi}{2} < \varphi < 0$ the conditional error is upper bounded by that of $\varphi = 0$ and we have

$$\begin{aligned} P_1(e|\varphi < 0) &< P_1\left(e|\varphi = 0\right) + p\left(\varphi < -\frac{\pi}{2}|\varphi < 0\right) \\ &= Q\left(\frac{\frac{1}{\sqrt{2}}}{\frac{1}{\sqrt{2}}\sigma_n}\right) + 2Q\left(\frac{\frac{\pi}{2}}{\sigma_\varphi}\right). \end{aligned}$$

In system 2, on the other hand, we use Jensen's inequality and strict convexity of $Q(\cdot)$ on $(0, \infty)$ to get the *lower* bound

$$\begin{aligned} P_2(e|\varphi < 0) &= \mathbb{E}_{\varphi<0}\left[P_2(e|\varphi)\right] \\ &> P_2\left(e|\mathbb{E}_{\varphi<0}[\varphi]\right) = Q\left(\frac{\frac{1}{\sqrt{2}} + \sqrt{\frac{16}{\pi^3}}\sigma_\varphi}{\frac{1}{\sqrt{2}}\sigma_n}\right) \end{aligned}$$

which implies,

$$\begin{aligned} \frac{1}{2}P_1(e|\varphi \geq 0) &< P_2(e) - \frac{1}{2}P_2(e|\varphi < 0) \\ &< Q\left(\frac{\frac{1}{\sqrt{2}}}{\sqrt{\frac{1}{2}\sigma_n^2 + \frac{8}{\pi^2}\sigma_\varphi^2}}\right) - \frac{1}{2}Q\left(\frac{\frac{1}{\sqrt{2}} + \sqrt{\frac{16}{\pi^3}}\sigma_\varphi}{\frac{1}{\sqrt{2}}\sigma_n}\right). \end{aligned}$$

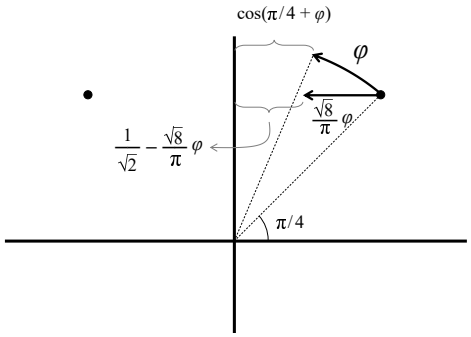

Fig. 11: Margin left for additive noise n after phase distortion and equivalent additive distortion.

1536-1276 (c) 2021 IEEE. Personal use is permitted, but republication/redistribution requires IEEE permission. See http://www.ieee.org/publications_standards/publications/rights/index.html for more information.
Authorized licensed use limited to: Univ of Calif Santa Barbara. Downloaded on June 24,2021 at 00:24:41 UTC from IEEE Xplore. Restrictions apply.

This article has been accepted for publication in a future issue of this journal, but has not been fully edited. Content may change prior to final publication. Citation information: DOI 10.1109/TWC.2021.3074911, IEEE Transactions on Wireless Communications

We therefore obtain an upper bound for the overall error rate as,

$$\begin{aligned}
P_1(e) &= \frac{1}{2}P_1(e|\varphi \geq 0) + \frac{1}{2}P_1(e|\varphi < 0) \\
&< \frac{1}{2}P_2(e|\varphi \geq 0) + \frac{1}{2}\left(Q\left(\frac{\frac{1}{\sqrt{2}}}{\frac{1}{\sqrt{2}}\sigma_n}\right) + 2Q\left(\frac{\frac{\pi}{2}}{\sigma_\varphi}\right)\right) \\
&< Q\left(\frac{1}{\sqrt{\sigma_n^2 + \frac{16}{\pi^2}\sigma_\varphi^2}}\right) \\
&+ \frac{1}{2}\left(Q\left(\frac{1}{\sigma_n}\right) - Q\left(\frac{1+\sqrt{\frac{32}{\pi^3}}\sigma_\varphi}{\sigma_n}\right)\right) + Q\left(\frac{\frac{\pi}{2}}{\sigma_\varphi}\right) \\
&= Q\left(\sqrt{\text{SNR}_{\text{eq}}}\right) \\
&+ \frac{1}{2}\left(Q\left(\sqrt{\text{SNR}}\right) - Q\left(\sqrt{\text{SNR}} + \sqrt{\frac{2\text{SNR}}{\pi\text{SNR}_\varphi}}\right)\right) \\
&+ Q\left(2\sqrt{\text{SNR}_\varphi}\right). \qquad (54)
\end{aligned}$$

□

APPENDIX B
COMPUTATIONS OF SPATIAL INNER PRODUCTS

Let $\mathbf{a}(\omega) = \left(1, e^{j\omega}, ..., e^{j(n-1)\omega}\right)^T$ denote the response of an n-element linear array to spatial frequency ω. Note that

$$\|\mathbf{a}(\omega)\|^2 = n. \qquad (55)$$

Applying this to (35) for $n = M$ gives us (36). The magnitude of the inner product between the responses for two different spatial frequencies ω_1 and ω_2, with $\Delta\omega = \omega_1 - \omega_2$, is given by

$$|\langle \mathbf{a}(\omega_1), \mathbf{a}(\omega_2)\rangle| = |1+e^{j\Delta\omega}+...+e^{j(n-1)\Delta\omega}| = \left|\frac{\sin n\Delta\omega/2}{\sin \Delta\omega/2}\right|$$

The corresponding normalized inner product is the magnitude of the well-known Dirichlet kernel:

$$\kappa_n(\Delta\omega) = \left|\frac{\sin n\Delta\omega/2}{n\sin \Delta\omega/2}\right| \qquad (56)$$

If ω_1, ω_2 are independent and uniform over $(-\pi, \pi)$, then modulo 2π, $\Delta\omega$ is uniform over $(-\pi, \pi)$. Squaring the $|\cdot|$ term in (B) and taking expectations, the contribution of cross-terms of the form $e^{jk\Delta\omega}$, where k is a nonzero integer, is zero. We therefore obtain

$$E\left[|\langle \mathbf{a}(\omega_1), \mathbf{a}(\omega_2)\rangle|^2\right] = n \qquad (57)$$

Applying this for $n = N_0$ gives us (37). We may also write this as

$$E\left[|\kappa_n(\Delta\omega)|^2\right] = \frac{1}{n} \qquad (58)$$

Applying this for $n = N$ gives us $\alpha = 1$ in (48).

To see what happens when we enforce a minimum spatial separation $2\pi/n$, note that $|x| \geq |\sin x|$, so that $\kappa_n(x) \geq |\frac{\sin(nx/2)}{nx/2}|$. We can now calculate that

$$\begin{aligned}
\frac{1}{2\pi}\int_{-2\pi/n}^{2\pi/n} \kappa_n^2(x)dx &\geq \frac{1}{2\pi}\int_{-2\pi/n}^{2\pi/n}\left|\frac{\sin(nx/2)}{nx/2}\right|^2 dx \\
&= \frac{1}{n\pi}\int_{-\pi}^{\pi}\left|\frac{\sin(u)}{u}\right|^2 du \geq \frac{0.90}{n}. \qquad (59)
\end{aligned}$$

Setting $n = N$, under the assumed minimum spatial separation of $\frac{2\pi}{N}$, we therefore obtain that $\mathbb{E}|\rho|^2 \leq \frac{0.1}{N}$,so that we may set $\alpha = 0.1$ in (48).

REFERENCES

[1] M. Abdelghany, A. A. Farid, U. Madhow, and M. J. Rodwell, "Towards all-digital mmwave massive MIMO: Designing around nonlinearities," in *2018 52nd Asilomar Conference on Signals, Systems, and Computers*. IEEE, 2018.

[2] S. Jacobsson, G. Durisi, M. Coldrey, U. Gustavsson, and C. Studer, "Throughput analysis of massive MIMO uplink with low-resolution ADCs," *IEEE Transactions on Wireless Communications*, vol. 16, no. 6, pp. 4038–4051, 2017.

[3] E. Björnson, J. Hoydis, M. Kountouris, and M. Debbah, "Massive MIMO systems with non-ideal hardware: Energy efficiency, estimation, and capacity limits," *IEEE Transactions on Information Theory*, vol. 60, no. 11, 2014.

[4] N. N. Moghadam, G. Fodor, M. Bengtsson, and D. J. Love, "On the Energy Efficiency of MIMO Hybrid Beamforming for Millimeter-Wave Systems With Nonlinear Power Amplifiers," *IEEE Transactions on Wireless Communications*, vol. 17, no. 11, pp. 7208–7221, 2018.

[5] M. Wu, D. Wübben, A. Dekorsy, P. Baracca, V. Braun, and H. Halbauer, "Hardware impairments in millimeter wave communications using OFDM and SC-FDE," in *20th International ITG Workshop on Smart Antennas*. VDE, 2016, pp. 1–8.

[6] D. Leeson, "A simple model of feedback oscillator noise spectrum," *proc. IEEE*, vol. 54, no. 2, pp. 329–330, 1966.

[7] B. Razavi, "A study of phase noise in CMOS oscillators," *IEEE journal of Solid-State circuits*, vol. 31, no. 3, 1996.

[8] A. Hajimiri and T. H. Lee, "A general theory of phase noise in electrical oscillators," *IEEE journal of solid-state circuits*, vol. 33, no. 2, pp. 179–194, 1998.

[9] A. Mehrotra, "Noise analysis of phase-locked loops," in *Proceedings of the 2000 IEEE/ACM international conference on Computer-aided design*. IEEE Press, 2000, pp. 277–282.

[10] Y. W. Kim and J. Du Yu, "Phase noise model of single loop frequency synthesizer," *IEEE Transactions on Broadcasting*, vol. 54, no. 1, pp. 112–119, 2008.

[11] F. Herzel, S. A. Osmany, and J. C. Scheytt, "Analytical phase-noise modeling and charge pump optimization for fractional-N PLLs," *IEEE Transactions on Circuits and Systems I: Regular Papers*, vol. 57, no. 8, pp. 1914–1924, 2010.

[12] S. Kalia, M. Elbadry, B. Sadhu, S. Patnaik, J. Qiu, and R. Harjani, "A simple, unified phase noise model for injection-locked oscillators," in *2011 IEEE Radio Frequency Integrated Circuits Symposium*. IEEE, 2011, pp. 1–4.

[13] M. R. Khanzadi, D. Kuylenstierna, A. Panahi, T. Eriksson, and H. Zirath, "Calculation of the performance of communication systems from measured oscillator phase noise," *IEEE Transactions on Circuits and Systems I: Regular Papers*, vol. 61, no. 5, pp. 1553–1565, 2014.

[14] E. Björnson, M. Matthaiou, and M. Debbah, "Massive MIMO with non-ideal arbitrary arrays: Hardware scaling laws and circuit-aware design," *IEEE Transactions on Wireless Communications*, vol. 14, no. 8, pp. 4353–4368, 2015.

[15] H. Thomas, V. Ranki *et al.*, "Phase noise in beamforming," *IEEE Transactions on Wireless Communications*, vol. 9, no. 12, pp. 3682–3689, 2010.

[16] R. Combes and S. Yang, "An approximate ml detector for MIMO channels corrupted by phase noise," *IEEE Transactions on Communications*, vol. 66, no. 3, pp. 1176–1189, 2017.

[17] Y.-F. Wang and J.-H. Lee, "A ZF-based precoding scheme with phase noise suppression for massive MIMO downlink systems," *IEEE Transactions on vehicular Technology*, vol. 67, no. 2, pp. 1158–1173, 2017.

1536-1276 (c) 2021 IEEE. Personal use is permitted, but republication/redistribution requires IEEE permission. See http://www.ieee.org/publications_standards/publications/rights/index.html for more information.
Authorized licensed use limited to: Univ of Calif Santa Barbara. Downloaded on June 24,2021 at 00:24:41 UTC from IEEE Xplore. Restrictions apply.

This article has been accepted for publication in a future issue of this journal, but has not been fully edited. Content may change prior to final publication. Citation information: DOI 10.1109/TWC.2021.3074911, IEEE Transactions on Wireless Communications

[18] X. Chen, A. Wolfgang, and T. Svensson, "Uplink multiuser MIMO-OFDM system in the presence of phase noises, power imbalance, and correlation," *Wireless Communications and Mobile Computing*, vol. 2018, 2018.

[19] Y.-F. Wang and J.-H. Lee, "A simple phase noise suppression scheme for massive MIMO uplink systems," *IEEE Transactions on Vehicular Technology*, vol. 66, no. 6, pp. 4769–4780, 2016.

[20] A. Pitarokoilis, S. K. Mohammed, and E. G. Larsson, "Uplink performance of time-reversal MRC in massive MIMO systems subject to phase noise," *IEEE Transactions on Wireless Communications*, vol. 14, no. 2, pp. 711–723, 2014.

[21] A. Pitarokoilis, E. Björnson, and E. G. Larsson, "Performance of the massive MIMO uplink with OFDM and phase noise," *IEEE Communications Letters*, vol. 20, no. 8, pp. 1595–1598, 2016.

[22] R. Krishnan, M. R. Khanzadi, N. Krishnan, Y. Wu, A. G. i Amat, T. Eriksson, and R. Schober, "Linear massive MIMO precoders in the presence of phase noise—a large-scale analysis," *IEEE Transactions on Vehicular Technology*, vol. 65, no. 5, pp. 3057–3071, 2015.

[23] R. Krishnan, M. R. Khanzadi, N. Krishnan, A. Amat, T. Eriksson, N. Mazzali, and G. Colavolpe, "On the impact of oscillator phase noise on the uplink performance in a massive MIMO-OFDM system," *arXiv preprint arXiv:1405.0669*, 2014.

[24] M. R. Khanzadi, *Phase Noise in Communication Systems–Modeling, Compensation, and Performance Analysis*. Chalmers University of Technology, 2015.

[25] A. Puglielli, G. LaCaille, A. M. Niknejad, G. Wright, B. Nikolić, and E. Alon, "Phase noise scaling and tracking in OFDM multi-user beamforming arrays," in *International Conference on Communications (ICC)*. IEEE, 2016, pp. 1–6.

[26] T. C. Schenk, X.-J. Tao, P. F. Smulders, and E. R. Fledderus, "On the influence of phase noise induced ICI in MIMO OFDM systems," *IEEE Communications Letters*, vol. 9, no. 8, pp. 682–684, 2005.

[27] D. Petrovic, W. Rave, and G. Fettweis, "Effects of phase noise on OFDM systems with and without PLL: Characterization and compensation," *IEEE Transactions on communications*, vol. 55, no. 8, pp. 1607–1616, 2007.

[28] S. Wu and Y. Bar-Ness, "OFDM systems in the presence of phase noise: consequences and solutions," *IEEE Transactions on Communications*, vol. 52, no. 11, pp. 1988–1996, 2004.

[29] P. Robertson and S. Kaiser, "Analysis of the effects of phase-noise in orthogonal frequency division multiplex (OFDM) systems," in *Proceedings IEEE International Conference on Communications ICC'95*, vol. 3. IEEE, 1995, pp. 1652–1657.

[30] M. H. Madani, A. Abdipour, and A. Mohammadi, "Analysis of performance degradation due to non-linearity and phase noise in orthogonal frequency division multiplexing systems," *IET communications*, vol. 4, no. 10, pp. 1226–1237, 2010.

[31] K. Sathananthan and C. Tellambura, "Performance analysis of an OFDM system with carrier frequency offset and phase noise," in *54th Vehicular Technology Conference (VTC)*, vol. 4. IEEE, 2001, pp. 2329–2332.

[32] L. Tomba, "On the effect of wiener phase noise in OFDM systems," *IEEE Transactions on communications*, vol. 46, no. 5, pp. 580–583, 1998.

[33] T. Pollet, M. Van Bladel, and M. Moeneclaey, "BER sensitivity of OFDM systems to carrier frequency offset and Wiener phase noise," *IEEE Transactions on communications*, vol. 43, pp. 191–193, 1995.

[34] A. G. Armada and M. Calvo, "Phase noise and sub-carrier spacing effects on the performance of an OFDM communication system," *IEEE Communications Letters*, vol. 2, no. 1, pp. 11–13, 1998.

[35] M. E. Rasekh, M. Abdelghany, U. Madhow, and M. Rodwell, "Phase noise analysis for mmwave massive MIMO: a design framework for scaling via tiled architectures," in *53rd Annual Conference on Information Sciences and Systems (CISS)*. IEEE, 2019, pp. 1–6.

[36] O. Momeni and E. Afshari, "High power terahertz and millimeter-wave oscillator design: A systematic approach," *IEEE Journal of Solid-State Circuits*, vol. 46, no. 3, pp. 583–597, 2011.

[37] M. Abdelghany, U. Madhow, and A. Tölli, "Beamspace Local LMMSE: An Efficient Digital Backend for mmWave Massive MIMO," in *20th International Workshop on Signal Processing Advances in Wireless Communications (SPAWC)*. IEEE, 2019, pp. 1–5.

[38] M. Abdelghany, U. Madhow, and M. Rodwell, "An Efficient Digital Backend for Wideband Single-Carrier mmWave Massive MIMO," in *2019 IEEE Global Communications Conference (GLOBECOM)*. IEEE, 2019.

Maryam Eslami Rasekh received her B.S. and M.S. degrees in Electrical Engineering from Isfahan University of Technology in 2007 and Sharif University of Technology in 2009, respectively. She joined the Wireless Communication and Sensornets Lab at University of California Santa Barbara as a visiting scholar in 2013 and received her Ph.D. from UC Santa Barbara in 2020. She is currently a postdoctoral researcher at UC Santa Barbara working with Prof. Madhow in the WCSL lab. Her research is mainly focused on millimeter wave communication, networking, and sensing, with emphasis on next generation networks and applications. Her past and current research in this area includes wave propagation and channel modeling, compressive channel estimation and beamforming, backhaul network optimization, signal processing and frontend design for multiuser massive MIMO systems, and massive MIMO radar.

Mohammed Abdelghany received his B.Sc. and M.Sc. degrees in Electrical Communications Engineering from Cairo University, Cairo, Egypt, in 2012 and 2016, respectively. In 2015, he was a visiting student with Prof. Katabi at MIT Computer Science & Artificial Intelligence Lab, Cambridge, USA. He is currently pursuing his Ph.D. in the Wireless Communication and Sensornets Lab at UCSB, Santa Barbara, USA. His research interests include signal processing, wireless communications, and design of digital VLSI circuits and systems.

Upamanyu Madhow is Distinguished Professor of Electrical and Computer Engineering at the University of California, Santa Barbara. His current research interests focus on next generation communication, sensing and inference infrastructures centered around millimeter wave systems, and on fundamentals and applications of robust machine learning. He received his bachelor's degree in electrical engineering from the Indian Institute of Technology, Kanpur, in 1985, and his Ph.D. degree in electrical engineering from the University of Illinois, Urbana-Champaign in 1990. He has worked as a research scientist at Bell Communications Research, Morristown, NJ, and as a faculty at the University of Illinois, Urbana-Champaign. Dr. Madhow is a recipient of the 1996 NSF CAREER award, and co-recipient of the 2012 IEEE Marconi prize paper award in wireless communications. He has served as Associate Editor for the IEEE Transactions on Communications, the IEEE Transactions on Information Theory, and the IEEE Transactions on Information Forensics and Security. He is the author of two textbooks published by Cambridge University Press, Fundamentals of Digital Communication (2008) and Introduction to Communication Systems (2014).

Mark Rodwell holds the Doluca Family Endowed Chair in Electrical and Computer Engineering at UCSB and directs the SRC/DARPA Center for Converged TeraHertz Communications and Sensing. His group develops nm and THz transistors, high-frequency ICs, and wireless communcations systems. He and his collaborators received the 2010 IEEE Sarnoff Award, the 2012 Marconi Prize Paper Award, the 1997 IEEE Microwave Prize, the 2009 IEEE IPRM Conference Award, and the 1998 European Microwave Conference Microwave Prize.

1536-1276 (c) 2021 IEEE. Personal use is permitted, but republication/redistribution requires IEEE permission. See http://www.ieee.org/publications_standards/publications/rights/index.html for more information.
Authorized licensed use limited to: Univ of Calif Santa Barbara. Downloaded on June 24,2021 at 00:24:41 UTC from IEEE Xplore. Restrictions apply.